J. Chem. Thermodynamics 90 (2015) 199–208

Contents lists available at ScienceDirect

J. Chem. Thermodynamics

journal homepage: www.elsevier.com/locate/jct

Thermodynamic investigation of $Na_2U_2O_7$ using Knudsen effusion mass spectrometry and high temperature X-ray diffraction

A.L. Smith [a,b,*], J.-Y. Colle [a], P.E. Raison [a], O. Beneš [a], R.J.M. Konings [a,*]

[a] European Commission, Joint Research Centre, Institute for Transuranium Elements, P.O. Box 2340, D-76125 Karlsruhe, Germany
[b] Department of Materials Science and Metallurgy, University of Cambridge, 27 Charles Babbage Road, Cambridge CB3 0FS, United Kingdom

ARTICLE INFO

Article history:
Received 20 March 2015
Received in revised form 17 June 2015
Accepted 22 June 2015
Available online 2 July 2015

Keywords:
Knudsen effusion mass spectrometry (KEMS)
(Solid + gas) equilibria
High temperature X-ray diffraction
Sodium uranate

ABSTRACT

The vaporization behavior and decomposition mechanism of $NaUO_3$ were studied using Knudsen effusion mass spectrometry. The temperature dependence of the sodium partial pressure over the ternary phase field $NaUO_3$–$Na_2U_2O_7$–UO_2 was measured for the first time: $\log(P_{Na}/Pa) = 10.98(\pm0.04) - 14,999(\pm50)/(T/K)$. The enthalpy of formation of α-$Na_2U_2O_7$ was moreover derived from second law analysis of the data at $\Delta_f H^o_m(\alpha\text{-}Na_2U_2O_7, cr, T = 298.15\ K) = -(3208.4 \pm 5.5)\ kJ \cdot mol^{-1}$, in very good agreement with the value reported in the literature from solution calorimetry. The existence of three polymorphs for $Na_2U_2O_7$ (α, β, and γ) was confirmed using high temperature X-ray diffraction. The two phase transitions occur above about $T = 600$ K, and around $T = 1323$ K, respectively. Our results were finally assessed with respect to similar vaporization studies carried out in neighboring ternary phase fields of the Na–U–O phase diagram.

1. Introduction

Considerable interest has existed since the 1960s for the characteristics of the sodium uranate phases because of their technological importance for Sodium-cooled Fast Reactors (SFRs). From safety perspectives, it is essential to have a thorough knowledge of the chemistry of the nuclear fuel-sodium coolant interaction as the two might come into contact in the event of a breach of the stainless steel cladding. (U,Pu) O_2 mixed oxide fuel is currently the preferred option for SFRs, and as such, the structural [1,2], thermodynamic [3–8], magnetic [9–11], and spectroscopic [12–19] properties of the Na-U-O and Na-Pu-O ternary compounds have been investigated in the past. The potential products of interaction are numerous: (Na_3UO_4, $NaUO_3$, Na_2UO_4, Na_4UO_5, $Na_2U_2O_7$, $Na_6U_7O_{24}$) [20–23,1,24,25], and (Na_2PuO_3, Na_3PuO_4, Na_6PuO_5, $Na_4Pu_2O_5$, Na_4PuO_5, Na_5PuO_6) [1,2,26] for the first and second systems, respectively, but not all well characterized.

Knudsen effusion mass spectrometry is a powerful technique for the study of the vaporization behavior, thermal stability, and decomposition mechanism of those phases at high temperatures [27–30]. Battles et al. [27] studied the Na–U–O system using combined Knudsen effusion mass loss (KEML) and Knudsen effusion mass spectrometry (KEMS). The authors looked at the dissociation path of Na_3UO_4 through Na(g) and O_2(g) vaporization, and derived the sodium and oxygen potentials over the five ternary phase fields Na–UO_2–Na_3UO_4, UO_2–$NaUO_3$–Na_3UO_4, $NaUO_3$–Na_4UO_5–Na_3UO_4, $NaUO_3$–Na_2UO_4–Na_4UO_5, and $NaUO_3$–Na_2UO_4–$Na_2U_2O_7$. Later, Jayanthi et al. [28] and Pankajavelli et al. [29] studied the $NaUO_3$–Na_2UO_4–$Na_2U_2O_7$ and $NaUO_3$–$Na_2U_2O_7$–$Na_6U_7O_{24}$ phase fields, combining KEML/KEMS and the transpiration technique with electro motive force (emf) measurements so as to derive the molar Gibbs energies of formation of $NaUO_3$ and $Na_6U_7O_{24}$.

In the present work, the decomposition path of $NaUO_3$ was investigated by Knudsen effusion mass spectrometry. The sodium potential was measured for the first time over the ternary phase field $NaUO_3$–$Na_2U_2O_7$–UO_2, and the enthalpy of formation of α-$Na_2U_2O_7$ was determined from second and third law treatment of the data. The polymorphism of $Na_2U_2O_7$ was moreover investigated using high temperature X-ray diffraction: the transitions to the β and γ phases suggested in the literature were confirmed, and the coefficients of thermal expansion of β-$Na_2U_2O_7$ were determined for the first time in the temperature range (748 to 1223) K.

* Corresponding authors at: European Commission, Joint Research Centre, Institute for Transuranium Elements, P.O. Box 2340, D-76125 Karlsruhe, Germany (A.L. Smith).

E-mail addresses: als77@cam.ac.uk (A.L. Smith), rudy.konings@ec.europa.eu (R.J.M. Konings).

http://dx.doi.org/10.1016/j.jct.2015.06.026
0021-9614/

2. Materials and methods

2.1. Materials

The $NaUO_3$ material was kindly provided by NRG (Nuclear Research and Consultancy Group, Petten, The Netherlands). α-$Na_2U_2O_7$ was synthesized as described in another publication by reaction between depleted uranium dioxide ($^{238}UO_2$ from JRC-ITU stocks) and sodium carbonate (Na_2CO_3 99.95%, Sigma) mixed in stoichiometric amounts [25]. The purity of the samples were checked using X-ray powder diffraction at room temperature and ICP-MS analysis (table 1). $NaUO_3$ crystallizes in the orthorhombic system, in space group *Pbnm*. The structure of α-$Na_2U_2O_7$ was recently re-assessed by IJdo et al. using neutron diffraction, and found monoclinic ($Z = 4$), in space group $P2_1/a$ [24], and not $P2_1$ as reported in [25]. The ICP-MS analyses yielded sodium to uranium molar ratios of (0.999 ± 0.011) at/at and (1.029 ± 0.011) at/at for $NaUO_3$ and α-$Na_2U_2O_7$, respectively. [1]

2.2. Mass spectrometric measurements

The experimental setup consists of a Knudsen effusion cell coupled to a quadrupole mass spectrometer QMG422 (Pfeiffer Vacuum GmbH), equipped with a cross beam electron bombardment ion source, an axial faraday cup, and a 90° second electron multiplier (SEM) detector connected to an electrometer. The mass spectrometer covers the range of (1 to 512) amu. The Knudsen cell is placed in a high temperature furnace heated by tungsten-coil heating elements, and is surrounded by seven cylindrical thermal shields (three in tungsten, four in tantalum). The furnace is placed in a high vacuum chamber (10^{-7} to 10^{-8} mbar). The whole apparatus, specifically designed to study radioactive materials, is placed in a 5 cm thick lead shielded glove box. A schematic drawing of the setup was given in another publication [30].

Experiments were carried out in tungsten cells under vacuum. The temperature was increased gradually at a heating rate of 10 K/min, and the species vaporizing from the $NaUO_3$ sample analyzed with the mass spectrometer at 30 eV ionization electron energy.

The vapor pressure of species i in the gas phase, P_i, is related to the intensity of the molecular beam recorded for the ion k formed from species i, I_{ik}^+, to the actual temperature, T, and to a sensitivity factor specific to ion k, S_{ik}, as expressed in equation (1) [31]:

$$P_i = I_{ik}^+ \cdot T / S_{ik}. \tag{1}$$

The temperature, T, was calibrated by measuring the melting points of standard materials (Zn, Cu, Fe, Pt, Al_2O_3), identified as small plateaus on the vapor pressure curve.

The sensitivity factor, S_{ik}, is furthermore related to an instrumental factor, K_g, independent of the ion detected, to the ion partial ionization cross-section, σ_{ik}, isotopic abundance, f_{ik}, and to the efficiency of the second electron multiplier, γ_{ik}, according to:

$$S_{ik} = K_g \cdot \sigma_{ik} \cdot \gamma_{ik} \cdot f_{ik}. \tag{2}$$

All isotopic contributions were added before treatment of the data, meaning f_{ik} equals unity. For atomic species, the partial and total ionization cross sections are identical. When molecular species are involved, fragment ions might be formed in the gas phase next to the parent ions, and should be accounted for in the data treatment. The relation between partial and total ionization cross sections is expressed as follows [32,31]:

$$\overline{\sigma_i} = \sigma_{ik}\left(1 + \frac{I^+_{frag\,j}/\gamma_{ik}}{I^+_{par\,k}/\gamma_{ij}} + \cdots + \frac{I^+_{frag\,n}/\gamma_{ik}}{I^+_{par\,k}/\gamma_{in}}\right), \tag{3}$$

where $\overline{\sigma_i}$ is the total ionization cross section for species i, σ_{ik} the partial ionization cross section for the ion k, $I^+_{par\,k}$ the intensity of the ionized parent k, $I^+_{frag\,j}$ and $I^+_{frag\,j}$ the intensities of the fragment ions j and n, and γ the multiplier yield for each ion.

Combining relations (1), (2) and (3), one can express the partial pressure of species i as a function of the total ionization cross section and intensities of the parent and fragment ions:

$$P_i = \frac{1}{K_g \cdot \overline{\sigma_i}} \cdot \left(\frac{I^+_{par\,k} \cdot T}{\gamma_{ik}} + \frac{I^+_{frag\,j} \cdot T}{\gamma_{ij}} + \ldots + \frac{I^+_{frag\,n} \cdot T}{\gamma_{in}}\right). \tag{4}$$

The atomic ionization cross-sections of sodium, uranium, and oxygen were estimated using the program SIGMA [31,33,34] and data of Mann [33]. The total ionization cross section of O_2 was taken from the experimental studies of Straub et al. [35]. The total ionization cross sections of Na_2O, UO, UO_2, and UO_3 were calculated using the modified additive rule, as described by Deutsch et al. [36,37] ($\sigma(UO) = 13.18 \cdot 10^{-16}$ cm^2, $\sigma(UO_2) = 11.41 \cdot 10^{-16}$ cm^2, $\sigma(UO_3) = 10.40 \cdot 10^{-16}$ cm^2 at 30 eV). Finally, the efficiency of the second electron multiplier was approximated to $\gamma_{ik} = \delta/M_{ik}^{1/2}$, where M_{ik} is the molar mass of ion k, and δ is a constant, following Grimley [38].

The instrumental factor, K_g, was estimated by vaporizing a known quantity of silver together with the sample. Silver vaporizes in the same temperature range as our studied material, has a well-known vapor pressure [39], and stays relatively inert in the system, which makes it an ideal reference material for calibration. It is vaporized completely at about $T = 1500$ K. The sensitivity factor for silver, S_{Ag}, and therefore instrumental factor, K_g, can be determined experimentally as a function of temperature, using the ion intensities I_{Ag^+} of the silver isotopes ^{107}Ag and ^{109}Ag and the vapor pressure data of Hultgren et al. [39]:

$$S_{Ag} = I_{Ag^+} \cdot T / P_{Ag} = K_g \cdot \sigma_{Ag} \cdot \gamma_{Ag} \cdot f_{Ag}. \tag{5}$$

Knowing S_{Ag}, the partial pressure of species i is deduced by combining equations (2), (4) and (5):

$$P_i = \frac{\overline{\sigma_{Ag}}}{S_{Ag} \cdot \overline{\sigma_i}} \cdot M_{Ag}^{-1/2} \left(I^+_{park} \cdot T \cdot M^{1/2}_{park} + I^+_{fragj} \cdot T \cdot M^{1/2}_{fragj} + \cdots + I^+_{fragn} \cdot T \cdot M^{1/2}_{fragn}\right). \tag{6}$$

The partial pressure P_i of species i at temperature T is also related, under Knuden-effusion conditions, to the mass loss G_i of species i over a duration δt via the Hertz–Knudsen equation [31]:

$$G_i = P_i \cdot s \cdot C \cdot \delta t \cdot \left(\frac{M_i}{2 \cdot \pi \cdot R \cdot T}\right)^{1/2}, \tag{7}$$

where s is the effusion orifice surface, C the Clausing factor, M_i the molar mass, T the temperature, and R the ideal gas constant equal to 8.314462 J · K^{-1} · mol^{-1}. The effusion orifice surface was calculated from its diameter. The expression of Santeler [40] for a cylindrical channel was used for the Clausing factor, as detailed in another publication [41].

The combination of equations (6) and (7) yields the following expression for the total mass effused $\Delta m_i = \sum G_i$ over a period of effusion $\Delta t = \sum \delta t$ (*i.e.* on a chosen number of time intervals):

$$\Delta m_i = H_i \cdot \sum \left(I^+_{park} \cdot T^{1/2} \cdot M^{1/2}_{park} + I^+_{fragj} \cdot T^{1/2} \cdot M^{1/2}_{fragj} + \ldots + I^+_{fragn} \cdot T^{1/2} \cdot M^{1/2}_{fragn}\right), \cdot \delta t$$
$$\text{with } H_i = \frac{\overline{\sigma_{Ag}}}{S_{Ag} \cdot \overline{\sigma_i}} \cdot \frac{s \cdot C}{(2 \cdot \pi \cdot R)^{1/2}} \cdot \left(\frac{M_i}{M_{Ag}}\right)^{1/2}. \tag{8}$$

[1] The uncertainties are expanded uncertainties $U = k \cdot u_c$ where u_c is the combined standard uncertainty estimated following the ISO/BIPM Guide to the Expression of Uncertainty in Measurement. The coverage factor is $k = 2$.

TABLE 1
Provenance and purity of the samples used in this study.

Formula	Source	State	Color	Mass fraction Purity
Na_2CO_3	Sigma	Powder	White	0.9995
UO_2	JRC-ITU stocks	Powder	Brown/black	> 0.998
$NaUO_3$	NRG	Powder	Brown	> 0.995
$Na_2U_2O_7$	Synthesized in-house	Powder	Orange	> 0.99

The latter expression can also be used to estimate the sensitivity factor for silver, S_{Ag}, from the data of the initial weight of silver, Δm_{Ag}, loaded in the Knudsen cell. This second method yielded values of S_{Ag} in very good agreement with the determination (5) using the data of Hultgren et al. [39].

The enthalpy of vaporization of silver, $\Delta_{vap}H^{\circ}_{m}(Ag, l, T)$, estimated in the present study with the second law of thermodynamics for the equilibrium $Ag(l) = Ag(g)$, was equal to (260.5 ± 2.1) kJ · mol^{-1} for an average temperature of 1310 K along the measurement. Extrapolated to room temperature, this yielded an enthalpy of sublimation at (279.7 ± 2.1) kJ · mol^{-1}, in very good agreement with the value suggested by Hultgren et al. $T = 298.15$ K, *i.e.* (284.1 kJ · mol^{-1}) [39].

Ionization efficiency curves were finally recorded at specific temperatures to get a better insight into the dissociation and ionization mechanisms of the species monitored. Isothermal scans of the ion intensities were obtained by increasing the cathodic voltage stepwise by 0.5 eV. The applied cathodic voltage was corrected as described previously [41,42] to give the effective electron energy with errors corresponding to a standard deviation of 1σ.

2.3. High temperature X-ray diffraction

The polymorphism of $Na_2U_2O_7$ was investigated by high temperature X-ray diffraction using a Bruker D8 X-ray diffractometer mounted with a curved Ge monochromator (111), a copper ceramic X-ray tube (40 kV, 40 mA), a Linx Eye position sensitive detector, and equipped with an Anton Paar HTK 2000 chamber. Measurements were conducted in air from room temperature up to 1373 K. The lattice parameters determined at each temperature with a Le Bail fit are listed in table 2. The temperature, measured with a thermocouple, was previously calibrated using the thermal expansion data of MgO [43]. The uncertainty on the temperature is estimated to be 20 K at 1473 K. The data were collected by step scanning in the angle range $10^{\circ} \leqslant 2\theta \leqslant 50^{\circ}$ for 6 h. Each temperature plateau was maintained at least 24 h (and at most 72 h), and continuous successive scans were collected during this time. The thermal expansion coefficients of $Na_2U_2O_7$ were derived from those measurements, as detailed in the Supplementary Information.

3. Results

3.1. Vaporization behavior of $NaUO_3$

The intensity signals recorded by the quadrupole mass spectrometer, while the $NaUO_3$ sample was heated together with silver up to $T = 2300$ K, are shown in figure 1a and figure 1b. We shall refer to regions A to C depicted on these figures throughout all this work.

The silver calibration signal grows from $T = (1040$ to $1455)$ K, at which point it diminishes suddenly meaning all the silver has evaporated. The signal of Na^+, detected around $T = 1170$ K, increases continuously up to $T = 1615$ K (figure 1a and figure 1b). A change in slope of the signal is observed around $T = 1550$ K, which defines the limit between regions A and B.

In region B, above $T = 1550$ K, the signals of O_2^+, NaO^+, and Na_2O^+ start to augment (figure 1b). All those signals drop at $T = 1615$ K together with Na^+. The signals of WO^+, WO_2^+, and WO_3^+ are also detected in this temperature range (figure 1a), indicating that the tungsten cell material is being oxidized [44,45].

Besides, the masses 292, 293, 294, and 296 appear in region A, which probably correspond to $Na_2WO_4^+$ (the tungsten having four isotopes ^{182}W, ^{183}W, ^{184}W, and ^{186}W). The masses 253, 254, 255, and 257 recorded in region B probably correspond to $NaWO_3^+$ (figure 1b). The occurrence of such signals suggests that sample and cell material react to form ternary sodium tungstate compounds. The intensities of the latter vapor species remain low, however, indicating a very limited process, that does not influence the measurement.

Finally, signals of U^+, UO^+, UO_2^+, and UO_3^+ appear around $T = 1755$ K, and develop steadily up to $T = 2300$ K when the measurement was stopped (region C). Such a behavior is typical of the vaporization process of uranium dioxide [42]. X-ray diffraction analysis of a sample heated in the Knudsen cell up to $T = 2016$ K, and quenched to room temperature, confirmed that only uranium dioxide was present after heating at this temperature. The cell parameter was found at $a = 0.5471(2)$ nm, in very good agreement with the literature for stoichiometric uranium dioxide [46].

TABLE 2
Evolution with temperature of the a, b, c, and β cell parameters, unit cell volume (Vol.), and density (ρ) of α-$Na_2U_2O_7$, β-$Na_2U_2O_7$, and γ-$Na_2U_2O_7$ measured at pressure $p = 9 \cdot 10^4$ Pa.

Temperature (K)	a/nm	b/nm	c/nm	β/°	Vol./nm^3	ρ/g · cm^3
α-$Na_2U_2O_7$	($Z = 4$)					
303	1.2778	0.7823	0.6880	111.28	0.6409	6.570
373	1.2802	0.7832	0.6885	111.23	0.6435	6.544
473	1.2840	0.7841	0.6889	111.21	0.6466	6.512
573	1.2877	0.7855	0.6895	111.11	0.6507	6.471
β-$Na_2U_2O_7$	($Z = 4$)					
748	1.2946	0.7894	0.6910	110.87	0.6598	6.382
823	1.2974	0.7902	0.6912	110.80	0.6624	6.357
923	1.3012	0.7911	0.6916	110.72	0.6659	6.324
1023	1.3051	0.7919	0.6919	110.64	0.6693	6.292
1123	1.3092	0.7929	0.6923	110.55	0.6729	6.258
1223	1.3130	0.7939	0.6926	110.48	0.6763	6.226
γ-$Na_2U_2O_7$	($Z = 3/2$)					
1323	0.3987(3)	0.3987(3)	1.8491(3)	90	0.2546	6.202

Standard uncertainties u are $u(T) = 20$ K, $u(a) = 0.0003$ nm, $u(b) = 0.0003$ nm, $u(c) = 0.0003$ nm, $u(\beta) = 0.05^{\circ}$.
u(Vol.) = 0.0005 nm^3, $u(\rho) = 0.005$ g · cm^{-3}, $u(p) = 2 \cdot 10^4$ Pa.

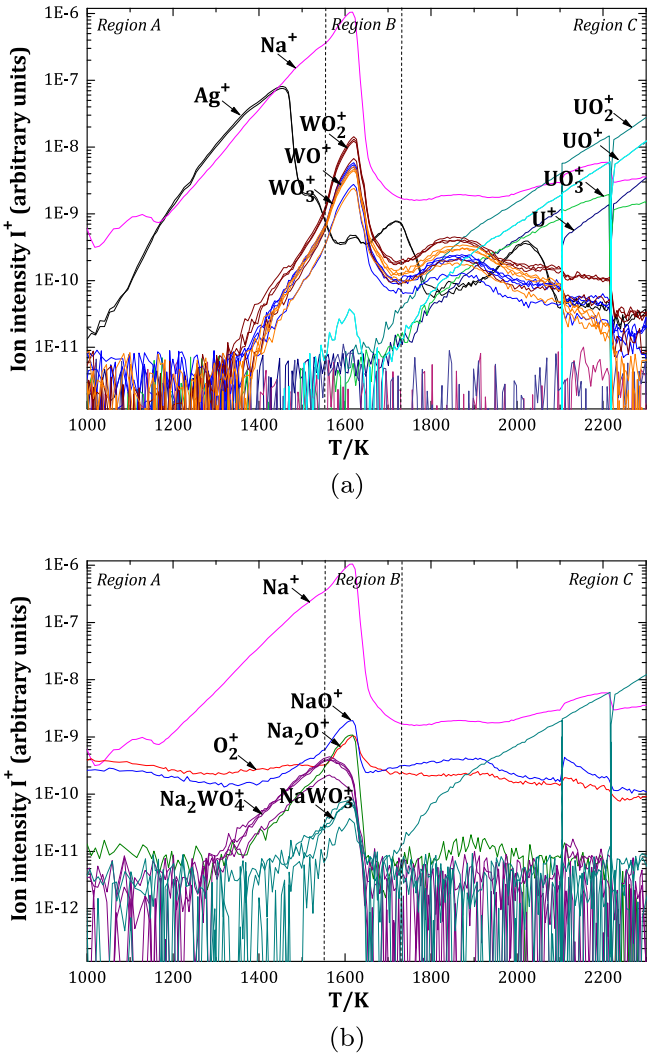

FIGURE 1. Intensity signals collected as a function of temperature for Na^+(23), Ag^+(107,109), WO^+(198,199,200,202), WO_2^+(214,215,216,218), WO_3^+(230,231,232,234), U^+(238), UO^+(254), UO_2^+(270), UO_3^+(286), O_2^+(32), NaO^+(39), Na_2O^+(62), $Na_2WO_4^+$(292,293,294,296), $NaWO_3^+$(253,254,255,257).

3.2. Ionization efficiency curves at T = 2105 K

Uranium dioxide is known to present a hypo- and hyper-stoichiometric homogeneity range, corresponding to the formula $UO_{2\pm x}$ [46]. Ionization efficiency curves, shown in the Supplementary Information, were hence recorded at $T = 2105$ K to determine the composition of the vapor phase, and corresponding stoichiometry of the uranium dioxide solid phase. The sudden drops in signal intensities visible on figure 1a and b, at $T = (2105$ and $2219)$ K respectively, correspond to two ionization efficiency curves measurements.

The appearance potential data recorded are listed in the Supplementary Information together with the associated ionization and dissociation mechanisms, and a comparison with literature data.

In the present work, the recorded U^+ and UO^+ signals come from the dissociation of UO_2(g) vapor species. UO_3^+ is moreover present at significant levels as shown in figure 1a, but its intensity rapidly diminishes as the temperature is increased, indicating a rapid reduction of the uranium dioxide material with temperature.

The partial pressures of the various vapor species were subsequently corrected for the dissociation processes. The vapor was found to be composed of 86.6% UO_2(g) and 13.4% UO_3(g) at $T = 2105$ K. The oxygen potential above the solid sample, which reflects the equilibrium between oxygen in the crystal lattice and oxygen in the gas phase, was estimated from the partial pressures of UO_2(g) and UO_3(g) as described in [47]. The sample's stoichiometry was finally estimated from the latter data using the thermodynamic model developed by Guéneau et al. [48]. The calculation led to a O/U ratio equal to (1.99 ± 0.01), confirming that the uranium dioxide formed at the end of region B was very close to stoichiometry, in agreement with the X-ray analysis performed on quenched samples.

4. Discussion

4.1. Decomposition mechanism of $NaUO_3$

High temperature X-ray diffraction measurements performed on the $NaUO_3$ material under helium [25] have evidenced the formation of $Na_2U_2O_7$ and UO_2 between $T = (1273$ and $1373)$ K. The corresponding decomposition reaction can be written as:

$$3NaUO_3(cr) = Na_2U_2O_7(cr) + UO_2(cr) + Na(g). \quad (9)$$

Na^+ is the only signal detected in region A around $T = 1170$ K during the Knudsen experiment. It corresponds to the direct ionization of Na(g) if we assume that reaction (9) is taking place in this temperature range. The onset of the decomposition reaction is found at slightly higher temperatures by X-ray diffraction. This is probably related to the different atmospheric conditions (helium at $P = 1$ bar in the X-ray diffraction measurements, vacuum at $P = (10^{-7}$ to $10^{-8})$ mbar in the Knudsen experiment). Moreover, the amount of $Na_2U_2O_7$ and UO_2 secondary phases formed up to $T = (1273$ to $1373)$ K are probably below detection levels in the X-ray diffraction measurements.

In region B, the increase of O_2^+, NaO^+, and Na_2O^+ signals alongside Na^+, suggests that $Na_2U_2O_7$ is further decomposing to Na_2O and UO_2 according to the reaction:

$$Na_2U_2O_7(cr) = 2UO_2(cr) + Na_2O(cr) + O_2(g). \quad (10)$$

At those temperature ranges sodium oxide vaporizes according to the following decomposition mechanisms [49,50]:

$$Na_2O(cr) = 2Na(g) + \frac{1}{2}O_2(g), \quad (11)$$

$$Na_2O(cr) = Na_2O(g), \quad (12)$$

$$Na_2O(cr) = NaO(g) + Na(g). \quad (13)$$

At any temperature, the resulting congruent vaporizing composition of sodium oxide imposed by effusion becomes $Na_{2+x}O$(cr) with the associated vaporization reaction [51]:

$$2Na_{2+x}O(cr) = 2Na(g) + \frac{1}{2}(1-2x)O_2(g) + Na_2O(g) + 2xNaO(g). \quad (14)$$

The value of x is very small, however, as sodium oxide has a very narrow homogeneity range [52], and can be considered negligible in the present study.

Na_2O^+ is formed by direct ionization of Na_2O(g). The NaO^+ signal comes from the dissociation of this same gaseous molecular species. The Na^+ signal recorded in region B probably has several contributions: mainly the direct ionization of Na(g), but also very minor contributions from dissociation of Na_2O(g). The latter was neglected in the present work.

The combination of equations (10) and (14) with $x = 0$ yields the following equilibrium reaction in region B:

$$Na_2U_2O_7(cr) = 2UO_2(cr) + Na(g) + \frac{1}{2}Na_2O(g) + \frac{5}{4}O_2(g). \quad (15)$$

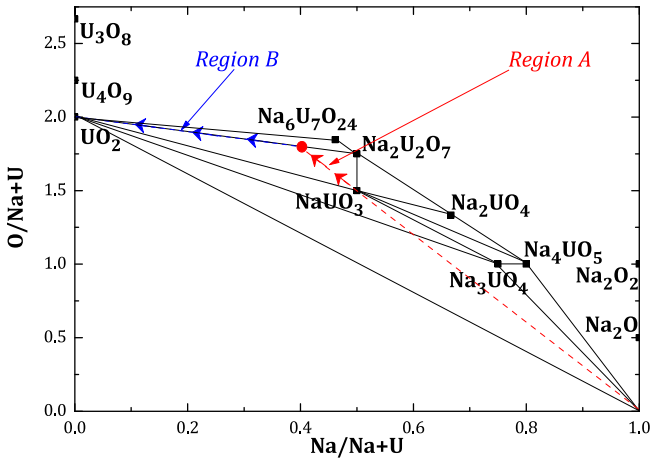

FIGURE 2. Evolution of the solid sample composition by effusion in the ternary Na–U–O phase diagram.

The disappearance of Na^+, NaO^+, Na_2O^+, and O_2^+ signals at the end of region B around T = 1620 K indicates the complete decomposition of $NaUO_3$ and $Na_2U_2O_7$ phases at this temperature. Region C finally corresponds to the sublimation of the uranium dioxide formed by effusion as detailed in the experimental section.

So as to confirm those decomposition mechanisms, the sodium mass loss was estimated with the Hertz–Knudsen relation (7), by integration of the G_{Na^+} signal along the measurement. The calculation yielded, at the end of region A, 30% of the total amount of sodium vaporized during the experiment, the remaining 70% vaporizing in region B. Those results, in very good agreement with equations (9) and (15), show that the decomposition of $NaUO_3$ in region A proceeds as written in equation (9) until all $NaUO_3$ has disappeared. In other words, the sample evolves by effusion in region A in the ternary phase field UO_2–$Na_2U_2O_7$–$NaUO_3$, while it evolves in region B on the pseudo-binary section UO_2–$Na_2U_2O_7$ (figure 2). The variance of the system is equal to 1 and goes to zero for a given temperature. This implies that at each temperature point the pressure is fixed, as well as the gas phase composition.

4.2. Derivation of the standard enthalpy of formation of α-$Na_2U_2O_7$

This is the first time the partial pressure of Na(g), P_{Na}, is measured in the ternary phase field $NaUO_3$–$Na_2U_2O_7$–UO_2. P_{Na} was derived using the Hertz–Knudsen equation (6) (table 3). Its temperature dependence can be represented by the following least-squares expression[2] over the temperature range (1292 to 1495) K:

$$\log(P_{Na}/Pa) = 10.98(\pm 0.04) - 14999(\pm 50)/(T/K). \quad (16)$$

The variation of the sodium partial pressure is compared in figure 3 to the ones measured in the neighboring phase fields $NaUO_3$–Na_2UO_4–$Na_2U_2O_7$, $NaUO_3$–Na_2UO_4–Na_4UO_5, $NaUO_3$–Na_3UO_4–Na_4UO_5, $NaUO_3$–Na_3UO_4–UO_2, and $NaUO_3$–$Na_2U_2O_7$–$Na_6U_7O_{24}$, using mass loss (KEML) and mass spectrometric Knudsen (KEMS) methods [27,28], and a thermogravimetric based transpiration technique [29]. The slope of our experimental curve is very similar to the ones reported by Battles et al. [27] and Pankajavelli et al. [29]. The absolute pressure stands between those measured for the ternary phase fields $NaUO_3$–Na_2UO_4–$Na_2U_2O_7$ and $NaUO_3$–Na_2UO_4–Na_4UO_5.

[2] The quoted uncertainties correspond to the standard deviation on the least-squares fitting.

TABLE 3
Sodium pressures derived from the Knudsen effusion mass spectrometry measurements.

T^a/K	P^b/Pa	T^a/K	P^b/Pa
1292	0.2484	1401	1.826
1298	0.2804	1408	2.057
1305	0.3130	1414	2.336
1312	0.3535	1421	2.618
1318	0.3978	1427	2.905
1325	0.4508	1433	3.248
1331	0.5131	1440	3.649
1338	0.5851	1447	4.079
1344	0.6618	1454	4.529
1351	0.7463	1461	5.173
1357	0.8447	1467	5.748
1364	0.9614	1471	6.170
1371	1.094	1476	6.735
1378	1.248	1481	7.458
1386	1.420	1489	8.226
1394	1.606	1495	9.104

[a] Standard uncertainties u are $u(T)$ = 10 K.
[b] Relative standard uncertainties u_r are $u_r(P)$ = 0.10.

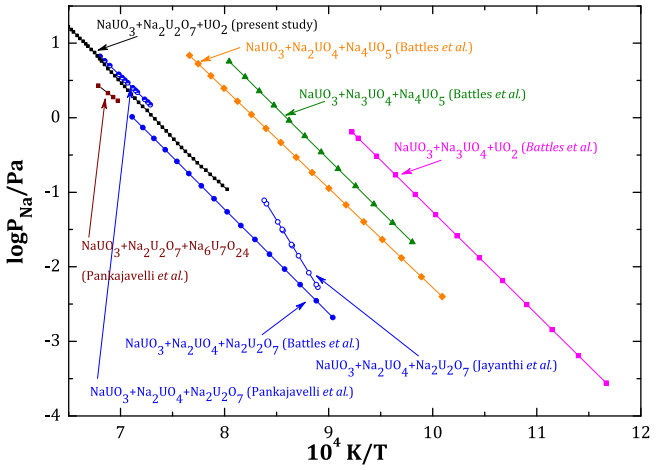

FIGURE 3. Sodium partial pressure measured in the ternary phase field $NaUO_3$–$Na_2U_2O_7$–UO_2 and comparison with literature data in neighboring phase fields of the Na–U–O phase diagram [27–29].

Considering the equilibrium reaction (9) in the temperature range (1170 to 1550) K, the enthalpy of reaction $\Delta_r H^o_m(T)$ is expressed as follows:

$$\Delta_r H^o_m(T) = \Delta_f H^o_m(Na_2U_2O_7, cr, T) + \Delta_f H^o_m(UO_2, cr, T) + \Delta_f H^o_m(Na, g, T) - 3\Delta_f H^o_m(NaUO_3, cr, T). \quad (17)$$

The thermodynamic functions of UO_2(cr), Na(g), and $NaUO_3$(cr) being well referenced in the literature, the present vapor pressure studies can be used to derive the enthalpy of formation of $Na_2U_2O_7$(cr).

The enthalpy of reaction was determined, as shown in figure 4, using the second law of thermodynamics (18) at an average temperature T_{ave} along the measurement:

$$d(\ln K_P)/d(1/T) = -\Delta_r H^o_m(T)/R. \quad (18)$$

K_P is the equilibrium constant of reaction (9) equal to:

$$K_P(T) = \{a_{Na_2U_2O_7} \cdot a_{UO_2}/a_{NaUO_3}\} \cdot \{P_{Na}/P^o\}, \quad (19)$$

where $a_{Na_2U_2O_7}$, a_{UO_2} and a_{NaUO_3} are the activities of solids equal to unity, P_{Na} the partial pressure of sodium, and P^o the standard partial pressure equal to 1 bar.

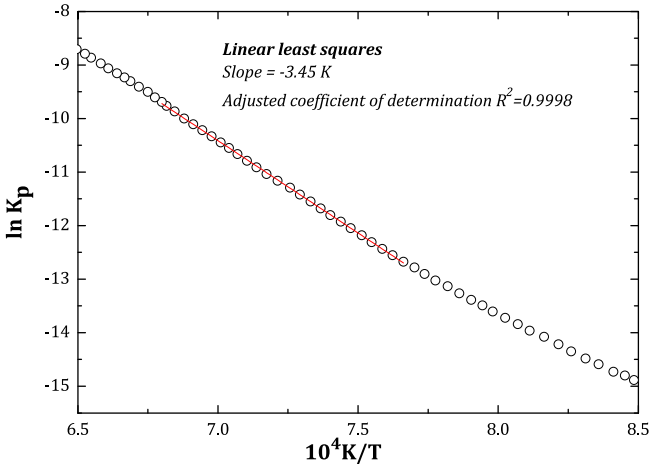

FIGURE 4. Linear fit of the curve $\ln K_p$ as a function of $1/T$ in region A.

The equilibrium constant was directly derived from the sodium partial pressure data. This analysis (figure 4) yielded an enthalpy of reaction in the range $T = (1300.8$ to $1470.5)$ K at (286.2 ± 2.3) kJ · mol^{-1} for the average temperature $T_{ave} = 1385.6$ K. This corresponds to an enthalpy of formation of $Na_2U_2O_7$ at $T = 1385.6$ K of $-(3396.2 \pm 5.5)$ kJ · mol^{-1}.

The enthalpy of reaction at $T = 298.15$ K was estimated from the experimental value at T_{ave}, and the theoretical enthalpy increment, $\Delta_r H^o_m(T_{ave}) - \Delta_r H^o_m(T = 298.15\ \text{K})$, the latter being calculated using the heat capacity data of $Na_2U_2O_7$(cr), $NaUO_3$(cr) [3], UO_2(cr) [53], and Na(g) [54] tabulated in the literature.

The calculation yielded an enthalpy of reaction at $T = 298.15$ K of (298.6 ± 2.3) kJ · mol^{-1}. The enthalpy of formation of α-$Na_2U_2O_7$ at $T = 298.15$ K was finally deduced from equation (17) at $\Delta_f H^o_m(\alpha - Na_2U_2O_7, \text{cr}, T = 298.15\ \text{K}) = -(3208.4 \pm 5.5)$ kJ · mol^{-1}, in very good agreement with solution calorimetry studies as detailed in Section 4.5.

This enthalpy of formation was also estimated using the third law method, which involves the use of the free energy function $\text{FEF}^o_m(T)$:

$$\text{FEF}^o_m(T) = -\left[G^o_m(T) - H^o_m(T = 298.15\ \text{K})\right]/T = S^o_m(T) - \left[H^o_m(T) - H^o_m(T = 298.15\ \text{K})\right]/T. \quad (20)$$

The standard enthalpy of reaction at $T = 298.15$ K was derived for each measurement temperature using the equation:

$$\Delta_r H^o_m(T = 298.15\ \text{K}) = -RT \ln K_P + T\Delta_r \text{FEF}^o_m(T). \quad (21)$$

The third law analysis, applied on the temperature range (1292 to 1481) K, yielded an enthalpy of reaction at $T = 298.15$ K of (271.6 ± 1.2) kJ · mol^{-1}, and correspondingly $\Delta_f H^o_m(\alpha - Na_2U_2O_7, \text{cr}, T = 298.15\ \text{K}) = -(3235.4 \pm 1.2)$ kJ · mol^{-1}.

The Gibbs energy of formation of $Na_2U_2O_7$ was finally derived for the temperature range (1292 to 1481) K by combining the Gibbs energy of reaction, $\Delta_r G^o_m(T) = -RT \ln K_P$, determined experimentally from the data of the sodium potential, together with the Gibbs energies of formation of UO_2(cr), Na(g), and $NaUO_3$(cr) tabulated in the literature:

$$\Delta_f G^o_m(Na_2U_2O_7, \text{cr}, T)/\text{kJ} \cdot \text{mol}^{-1} = -3402.6 + 0.78886(T/\text{K}) \quad (T = 1292 \text{ to } 1481\ \text{K}). \quad (22)$$

Those Gibbs energy values are about 30 kJ · mol^{-1} lower than the value recommended in the literature, however [3], and than the data of Pankajavelli et al. [29], obtained with the emf method over the temperature range (812 to 1101) K, and extrapolated to higher temperatures, as shown in figure 5. This discrepancy as well as the difference between the second and third law results are explained in Section 4.5.

4.3. Study of region B

The enthalpy of formation of $Na_2U_2O_7$ can also be derived from the equilibrium reaction (15) using an analogous procedure in region B. The contributions of the ionized species NaO^+ and Na_2O^+ were added so as to account for the partial pressure of Na_2O(g), while the partial pressures of Na(g) and O_2(g) were directly derived from the signals of Na^+ and O_2^+, respectively.

The values obtained in this temperature range for the enthalpy of formation of α-$Na_2U_2O_7$ by second and third law analyses agreed very well between each other, but were found about 70 kJ · mol^{-1} higher than expected [3]. In this temperature range, the signals of WO^+, WO_2^+, and WO_3^+ are detected at significant levels following the oxidation of the tungsten cell material. The equilibrium reaction, probably more complex than written in (15), should account for the tungsten oxide species. The experimental results obtained in this temperature range can hence unfortunately not be exploited for an accurate determination of the enthalpy of formation of $Na_2U_2O_7$, as the measured oxygen pressure does not reflect the equilibrium (15).

4.4. Polymorphism of $Na_2U_2O_7$

The heat capacity function of $Na_2U_2O_7$ recommended in the literature [3], and used in the previous section, was derived from the enthalpy increment data obtained by Cordfunke et al. over the temperature range (390 to 926) K using drop calorimetry [55,3]. The authors claimed the existence of a reversible phase transition from α-$Na_2U_2O_7$ to β-$Na_2U_2O_7$ above about 600 K, and from β-$Na_2U_2O_7$ to γ-$Na_2U_2O_7$ around $T = 1348$ K, which they observed with a high temperature X-ray Guinier camera. The exact temperature of the transitions were not determined [56,55], however, and the corresponding X-ray diffraction patterns and crystal structures were not reported. IJdo et al. could solve the structure of the β phase using high temperature neutron diffraction. They reported a monoclinic unit cell ($Z = 4$), in space group $C2/m$, with lattice parameters at 773 K: $a = 1.2933(1)$ nm, $b = 0.7887(1)$ nm, $c = 0.69086(8)$ nm, and $\beta = 110.816(10)°$.

The data of the experimental enthalpy increments as reported by Cordfunke et al. over the ranges $T = (390$ to $540)$ K (α-form) and (681 to 926) K (β-form), as well as the suggested fitting equations are shown in figure 6a and figure 6b. The enthalpy increment associated with the transition should be very small according to those results (around 1.6 kJ · mol^{-1} at $T = 600$ K). Cordfunke et al. reported very slow kinetics for this phase transition. But in their experiment the sample was kept several hours in a closed container before being "dropped" at $T = 298$ K, which should allow the formation of the equilibrium phase of the compound at each temperature point.

High temperature X-ray diffraction measurements were performed in the present work to gain further insight into the $\alpha \rightarrow \beta$ and $\beta \rightarrow \gamma$ transitions. The α-$Na_2U_2O_7$ material was heated under helium up to $T = 1073$ K as reported in another publication [25]. These data were re-assessed in light of the recent structure determination by IJdo et al. who assigned a monoclinic structure, in space group $P2_1/a$, and not $P2_1$ to the α form of the compound. The evolution of the lattice parameters with temperature is listed in table 2 and shown in the Supplementary Information.

Besides, the α-$Na_2U_2O_7$ material was heated at $T = 1100$ K for 24 h, plus $T = 793$ K for 48 h, before being quenched below $T = 77$ K in liquid nitrogen. The X-ray diffraction pattern obtained after the quenching experiment is shown in figure 7b together with

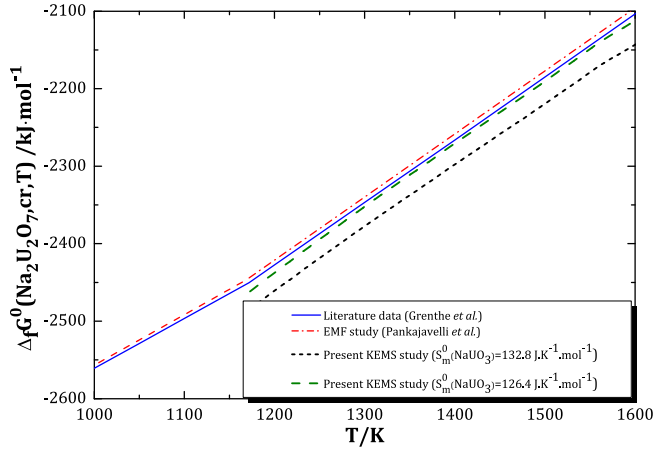

FIGURE 5. Gibbs energy of formation of $Na_2U_2O_7$ as estimated from the present study, and comparison with the literature data of Grenthe *et al.* [3,4], and emf study of Pankajavelli *et al.* [29].

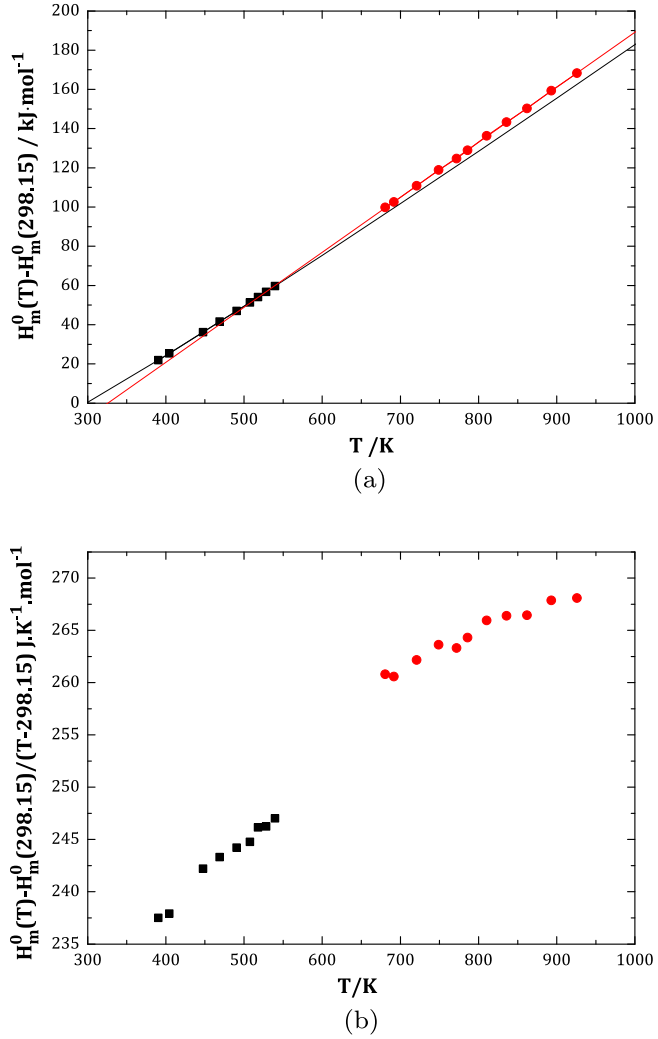

FIGURE 6. (a) Enthalpy increments data of $Na_2U_2O_7$ as reported by Cordfunke *et al.* [55] in the α (T = 390 to 540 K) (■) and β (T = 681 to 926 K) (●) ranges, and fitting equations. (b) Reduced enthalpy increments for the α (T = 390 to 540 K) (■) and β (T = 681 to 926 K) (●) ranges.

the one for the α form of the compound (figure 7a). This pattern does not correspond to pure β as the authors had expected, but to a mixture of α and β.

The quenched sample was subsequently heated from room temperature up to 1323 K under air. Up to T = 573 K, no significant change was observed in the X-ray diffraction patterns (shown in the Supplementary Information), except for a shift to lower 2θ values following the expansion of the unit cell. At T = 623 K, the α phase started to disappear and transform to β. The transformation was complete at T = 748 K only, and after 72 h of continuous successive scans at this temperature, confirming the slow kinetics of the $\alpha \rightarrow \beta$ transition. No further phase change was observed from T = (748 to 1223) K. But an increase in intensity was clearly visible, sign of an improvement of the sample's crystallinity. The evolution of the lattice parameters of β-$Na_2U_2O_7$ in this temperature range is listed in table 2. The X-ray diffraction pattern of the β phase collected at T = 1223 K is also shown in figure 7c. As IJdo et al. points out, α and β have closely related crystal structures. The diffraction patterns show only small changes, corresponding to a similarly little change in entropy, as reflected by the small values of the enthalpies of transition $\Delta_{tr}S^o_m(T_{tr}) = \Delta_{tr}H^o_m(T_{tr})/T_{tr}$ (around 1.6 kJ · mol^{-1} at T = 600 K for the α–β transition, and reported at 2.7 kJ · mol^{-1} at T = 1322 K for the β–γ transition [22]).

The phase transition to γ-$Na_2U_2O_7$ occurred between (1223 and 1323) K (figure 7). This transition was rapid, by contrast with the previous one. The γ compound is rhombohedral (Z = 3/2), in space group $R\bar{3}m$, and corresponds to the phase synthesized by Gasperin [57] at T = 1473 K. Gasperin managed inadvertently to synthesize single crystals of $Na_2U_2O_7$ while trying to make single crystals of UNb_3O_{10} in an excess of Na_2CO_3, and probably quenched this phase down to room temperature. A Le Bail fit was performed at T = 1323 K, yielding cell parameters at a = 0.3987(3) nm and c = 1.8491(3) nm. A complete structural study is out of the scope of the present work, and should be addressed in future studies.

Upon cooling at T = 923 K, the material transformed back to a mixture of α and β phases (X-ray diffraction patterns shown in the Supplementary Information), confirming the reversibility of the $\beta \rightarrow \gamma$ transition. All of the reflections appeared shifted to higher angles compared to the heating ramp, however, probably due to a slight lifting of the powder with temperature cycling. The final pattern obtained at room temperature, after complete cooling, corresponded to a phase mixture between α and β.

This experiment therefore confirms the existence of two phase transitions in $Na_2U_2O_7$, the first one occurring between

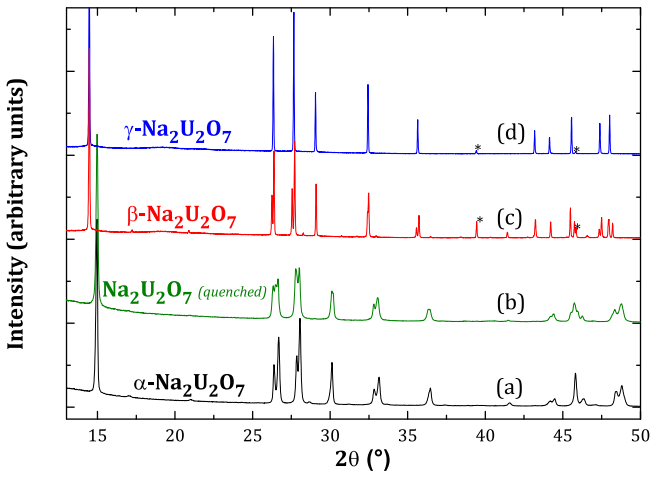

FIGURE 7. X-ray diffraction patterns of (a) α-$Na_2U_2O_7$ (collected at room temperature), (b) of the quenched phase obtained from α-$Na_2U_2O_7$ after heating at T = (1100 and 793) K followed by quenching in liquid nitrogen (collected at room temperature), (c) of β-$Na_2U_2O_7$ collected at T = 1223 K, and (d) of γ-$Na_2U_2O_7$ collected at T = 1323 K. *Denotes the reflections associated with the platinum heating strip.

TABLE 4
Enthalpy of formation of α-$Na_2U_2O_7$ at T = 298.15 K.

References	Method	$\Delta_f H^o_m(\alpha - Na_2U_2O_7, cr, T = 298.15\ K)/kJ \cdot mol^{-1}$
Cordfunke *et al.* [23,58,3]	Solution Calorimetry	−3196.1 ± 3.9
Cordfunke *et al.* [55]	Solution calorimetry	−3194.7 ± 1.4
Tso *et al.* [59]	Solution calorimetry	−3203.8 ± 2.8
Battles *et al.* [27]	KEML + KEMS	−3074.4 ± 31.4
Guillaumont *et al.* [4]	Review	**−3203.8 ± 4**
Present work	KEMS (second law)	**−3208.4 ± 5.5**[a]
	KEMS (third law)	−3235.4 ± 1.2[a]

Selected values are shown in bold.
[a] The uncertainties are standard uncertainties.

T = (573 and 623) K, and the second one between T = (1223 and 1323) K. This is the first time that the rhombohedral phase synthesized by Gasperin [57] is identified as the high temperature γ modification of $Na_2U_2O_7$, and that coefficients of thermal expansion are reported for β-$Na_2U_2O_7$. Details regarding the determination of those coefficients are given in the Supplementary Information. For α-$Na_2U_2O_7$, in space group $P2_1/a$, these were derived at: $\alpha_a = 28.8 \cdot 10^{-6}\ K^{-1}$, $\alpha_b = 14.8 \cdot 10^{-6}\ K^{-1}$, $\alpha_c = 7.9 \cdot 10^{-6}\ K^{-1}$, and $\alpha_\beta = -5.3 \cdot 10^{-6}\ K^{-1}$ in the temperature range (298 to 573) K. For β-$Na_2U_2O_7$, in space group $C2/m$, they were estimated at: $\alpha_a = 30.5 \cdot 10^{-6}\ K^{-1}$, $\alpha_b = 12.0 \cdot 10^{-6}\ K^{-1}$, $\alpha_c = 4.9 \cdot 10^{-6}\ K^{-1}$, and $\alpha_\beta = -7.4 \cdot 10^{-6}\ K^{-1}$ in the temperature range (748 to 1223) K.

The present data treatment of the Knudsen effusion mass spectrometry measurements takes into account the α–β phase transition, but does not consider the γ form since no thermodynamic functions were reported for the latter phase in the literature. A new calorimetric study covering temperatures above 1323 K would be required to complete the data of Cordfunke et al. and especially to assess the heat capacity function of γ-$Na_2U_2O_7$ [55,3].

4.5. Discussion

The enthalpies of formation of α-$Na_2U_2O_7$, obtained by second and third law analyses in region A, are compared in table 4 to the data reported in the literature. Our second law result, −(3208.4 ± 5.5) kJ · mol^{-1}, is in very good agreement with the values derived from solution calorimetry by Cordfunke et al. −(3196.1 ± 3.9) kJ · mol^{-1} [23,58,3], −(3194.7 ± 1.4) kJ · mol^{-1} [55,3], and with the value recommended in [4] **-(3203.8 ± 4) kJ· mol^{-1}** obtained for a high purity sample prepared by thermal decomposition in oxygen atmosphere of $NaUO_2(CH_3COO)_3$ [59]. The third law analysis yields a value that is about 30 kJ · mol^{-1} too low, however. It is unlikely that this discrepancy comes from the absolute values of the sodium partial pressures in region A, as these would need to be about 15 times lower to yield the expected enthalpy value for α-$Na_2U_2O_7$. This is excluded given the very good agreement with the sodium pressures measured in neighboring phase fields.

The discrepancy probably originates from a poor description of the free energy function of either $Na_2U_2O_7$ or $NaUO_3$. It is suggested that the entropy value of $NaUO_3$ reported in the literature at $S^o_m(NaUO_3, cr, T = 298.15\ K)$ = (132.8 ± 0.4) J · K^{-1} · mol^{-1} [60] might be overestimated. For comparison, the entropy value estimated with Neumann–Kopp's rule from the data of UO_2 [53], UO_3 [53], and Na_2O [61] is equal to 124.1 J · K^{-1} · mol^{-1}. The difference with the value reported by Lyon *et al.* [60] (8.7 J · K^{-1} · mol^{-1}) is rather large. When considering the value $S^o_m(NaUO_3, cr, T = 298.15\ K)$ = 126.4 J · K^{-1} · mol^{-1}, the standard enthalpy of formation derived by third law method, $\Delta_f H^o_m(\alpha - Na_2U_2O_7, cr, T = 298.15\ K)$ = −(3208.7 ± 0.3) kJ · mol^{-1}, gives the same result as the second law. Moreover, when applying this same correction, the Gibbs energy of formation of $Na_2U_2O_7$ is derived at:

$$\Delta_f G^o_m(Na_2U_2O_7, cr, T)/kJ \cdot mol^{-1} = -3402.6 + 0.8082(T/K)\ (1292\ \text{to}\ 1481\ K), \quad (23)$$

in much better agreement with the recommended literature data [3,4], and emf study of Pankajavelli *et al.* [29] as shown in figure 5.

The low temperature specific heat of $NaUO_3$ was measured by Lyon et al. using adiabatic calorimetry [60]. The compound revealed a non-isothermal peak at (31 ± 1) K related to antiferromagnetic ordering, as later confirmed by magnetic susceptibility, Electron Spin Resonance, and neutron diffraction measurements [62,63,9]. An eventual error in the derivation of the standard entropy could not be identified from their reported experimental data. But their sample, prepared by hydrogen reduction of $Na_2U_2O_7$ and characterized by chemical analysis, infrared spectroscopy, and with Debye–Scherrer X-ray powder photographs, might have contained some small impurity. A possible $Na_2U_2O_7$ contamination was detected from the infrared spectrum, but the authors estimated it to be very low (0.5 wt%), so that no corrections were made to the heat capacity values. Impurities below 5 wt% such as $Na_2U_2O_7$, Na_2O, or Na, would probably not have been detected with the Debye–Scherrer technique, however, and would have been very difficult to quantify accurately by chemical analysis or infrared spectroscopy. Given that the third law determination raises some doubts about the tabulated thermodynamic entropy of $NaUO_3$, we recommend in the present work the second law value, estimated independently of the latter data: $\Delta_f H^o_m(\alpha - Na_2U_2O_7, cr, T = 298.15\ K)$ = −(3208.4 ± 5.5) kJ · mol^{-1}.

When compared with the vapor pressure studies of Battles et al. [27], the present investigations have the advantage of not requiring the determination of the oxygen potential in the ternary phase field, which can be quite a complex process subject to significant uncertainty. The enthalpy of formation as suggested by Battles et al. [27] for $Na_2U_2O_7$ using combined KEML and KEMS analyses is quite far from the recommended value (table 4). In their work the sodium potential was measured directly and is relatively accurate, but the oxygen potential was calculated indirectly through a number of steps, the uncertainty on the first step being non negligible. As the oxygen potential was too low in most ternary phase fields for direct measurement except one ($NaUO_3$–Na_2UO_4–$Na_2U_2O_7$), it was estimated for each three-phases region from the data of the latter phase field and appropriate equilibrium dissociation reactions between Na(g), O_2(g), and solid phases common to neighboring phase fields. This calculation was subject to rather large errors, which explains the rather poor agreement with solution calorimetry studies.

The same problem occurred for the enthalpy determination of $NaUO_3$ as shown in table 5. Battles et al. obtained −(1440.1 ± 17.6) kJ · mol^{-1} instead of the value recommended from solution

TABLE 5
Enthalpy of formation of $NaUO_3$ at $T = 298.15$ K.

References	Method	$\Delta_f H^o_m(NaUO_3, cr, T = 298.15\ K)/kJ \cdot mol^{-1}$
Cordfunke and Loopstra [23]	Solution calorimetry	-1497.6 ± 4.9
Cordfunke and Ouweltjes [64]	Solution calorimetry	-1494.6 ± 1.7
O'Hare and Hoekstra [65,3]	Solution calorimetry	-1520.5 ± 3.3
Battles *et al.* [27]	KEML + KEMS	-1440.1 ± 17.6
Jayanthi *et al.* [28]	KEML + KEMS	-1481.4 ± 13.4
Pankajavelli *et al.* [29]	Transpiration	-1496.7 ± 0.5
Guillaumont *et al.* [4]	Review	$\mathbf{-1494.9 \pm 10}$

Selected values are shown in bold.

calorimetry $-(1494.9 \pm 10)\ kJ \cdot mol^{-1}$ [4]. One solution to avoid such issues is to use a complementary technique such as emf for determining the oxygen potential as done in the work of Jayanthi et al. [28] and Pankajavelli et al. [29].

Jayanthi et al. [28] worked in the $NaUO_3$–Na_2UO_4–$Na_2U_2O_7$ ternary phase field (over the $T = (1117$ to $1290)$ K temperature range) with a (3:1:2) mixture. The sodium and oxygen potentials corresponding to the equilibrium reaction (24) were estimated with the Knudsen effusion mass spectrometry and emf techniques respectively:

$$3NaUO_3(cr) + Na_2UO_4(cr) + \frac{1}{2}O_2(g) = 2Na_2U_2O_7(cr) + Na(g). \quad (24)$$

The enthalpy of formation was determined from second and third law treatment, using the thermodynamic functions of Na_2UO_4(cr), $Na_2U_2O_7$(cr), and Na(g) tabulated in the literature. The values obtained are $-(1481.4 \pm 13.4)\ kJ \cdot mol^{-1}$, and $-(1476.7 \pm 13.4)\ kJ \cdot mol^{-1}$, *i.e.* in rather good agreement with the literature, even though about 15 $kJ \cdot mol^{-1}$ lower than the recommended value.

Pankajavelli et al. [29] worked with the transpiration technique in the same ternary phase field, but with an equimolar mixture, based on the equilibrium reaction (25) for the temperature range (1368 to 1470) K:

$$NaUO_3(cr) + Na_2UO_4(cr) = Na_2U_2O_7(cr) + Na(g). \quad (25)$$

The authors derived the Gibbs energy of formation of $NaUO_3$ in the temperature range (1368 to 1470) K, by combining the experimental data of the sodium potential obtained with the transpiration technique, together with the Gibbs energy of formation of $Na_2U_2O_7$, $\Delta_f G^o_m(Na_2U_2O_7, cr, T)$, obtained from emf studies, and with $\Delta_f G^o_m(Na_2UO_4, cr, T)$, and $\Delta_f G^o_m(Na, g, T)$ tabulated in the literature. The authors subsequently derived the enthalpy of formation at $T = 298.15$ K by third law analysis using the experimental Gibbs energy function of $NaUO_3$ together with the values of the free energy functions of $NaUO_3$(cr), Na(cr), U(cr), and O_2(g) given in the literature. As shown in table 5 the agreement with solution calorimetry data is very good.

5. Conclusion

The present work reports for the first time the sodium partial pressure over the ternary phase field $NaUO_3$–$Na_2U_2O_7$–UO_2, hence complementing similar vaporization studies carried out in neighboring phase fields of the Na–U–O phase diagram. The enthalpy of formation of α-$Na_2U_2O_7$ has also been derived by second law analysis at $\Delta_f H^o_m(\alpha - Na_2U_2O_7, cr,\ T = 298.15\ K) = -(3208.4 \pm 5.5)\ kJ \cdot mol^{-1}$, in very good agreement with solution calorimetry studies. The third law analysis has questioned the reported entropy value for $NaUO_3$, however, with the possibility of a slight overestimation. Besides, high temperature X-ray diffraction studies have allowed to clarify the polymorphism of $Na_2U_2O_7$: α, monoclinic in space group $P2_1/a$, transforms to β, monoclinic in space group $C2/m$ above about $T = 600$ K, and to γ, hexagonal in space group $R\bar{3}m$, between $T = (1223$ and $1323)$ K. The coefficients of thermal expansion of α and β have also been derived. The present method is finally quite promising for the thermodynamic investigation of the poorly characterized Na–Np–O and Na–Pu–O ternary systems, and especially for the determination of the enthalpies of formation of sodium neptunates and sodium plutonates, for which other investigation techniques such as solution calorimetry are not always available, as long as no oxygen is formed, or supposing the determination of the oxygen potential is either possible directly [30], or available from complementary techniques such as emf.

Acknowledgments

The authors would like to express their gratitude to G. Pagliosa and D. Bouëxière for the collection of the X-ray diffraction data, and to the Analytical Services of the Institute for Transuranium Elements for performing the ICP-MS analysis. They also thank the 7^{th} Framework Program of the European Commission, and the Joint Advanced Severe Accidents Modelling and Integration for Na-cooled neutron reactors (JASMIN) programme (N°295803 in FP7). ALS acknowledges the European Commission and the Ras al Khaimah Centre for Advanced Materials for funding her PhD studentship. ALS would finally like to thank Prof. A.K. Cheetham from the Department of Materials Science and Metallurgy of the University of Cambridge for the fruitful discussions, and for his strong and continuous support.

Appendix A. Supplementary data

Supplementary data associated with this article can be found, in the online version, at http://dx.doi.org/10.1016/j.jct.2015.06.026.

References

[1] S. Pillon. Etude des diagrammes de phases U-O-Na, Pu-O-Na et U, Pu-O-Na (PhD thesis), Université Du Languedoc, 1989.
[2] H. Kleykamp, KfK 4701 (1990) 31.
[3] I. Grenthe, J. Fuger, R.J.M. Konings, R.J. Lemire, A.B. Muller, C. Nguyen-Trung Cregu, H. Wanner, Chemical Thermodynamics of Uranium. OECD Nuclear Energy Agency, Data Bank, Issy-les-Moulineaux (France), 1992.
[4] R. Guillaumont, T. Fanghänel, J. Fuger, I. Grenthe, V. Neck, D.A. Palmer, M.H. Rand, Update on the Chemical Thermodynamics of Uranium, Neptunium, Plutonium, Americium & Technetium, OECD Nuclear Energy Agency, Data Bank, Issy-les-Moulineaux (France), 2003.
[5] R.J. Lemire, J. Fuger, H. Nitsche, P. Potter, M.H. Rand, J. Rydberg, K. Spahiu, J.C. Sullivan, W.J. Ullman, P. Vitorge, H. Wanner, Chemical Thermodynamics of Neptunium and Plutonium, OECD Nuclear Energy Agency, Data Bank, Issy-les-Moulineaux (France), 2001.
[6] M.A. Mignanelli, P.E. Potter, Thermochim. Acta 129 (1988) 143–160.
[7] M.A. Mignanelli, P.E. Potter, J. Nucl. Mater. 130 (1985) 289–297.
[8] M.A. Mignanelli, P.E. Potter, J. Nucl. Mater. 125 (1984) 182–201.
[9] S. Van den Berghe, A. Leenaers, C. Ritter, J. Solid State Chem. 177 (2004) 2231–2236.
[10] E. König, C. Rudowicz, V.P. Desai, J. Chem. Phys. 78 (9) (1983) 5764–5771.
[11] B. Kanellakopulos, C. Keller, R. Klenze, A.H. Stollenwerk, Physica B 102 (1980) 221–225.

[12] M. Bickel, B. Kanellakopulos, B. Powietzka, J. Less Common Met. 170 (1991) 161–169.
[13] W.T. Carnall, S.J. Neufeldt, A. Walker, Inorg. Chem. 4 (12) (1965) 1808–1813.
[14] H.R. Hoekstra, J. Inorg. Nucl. Chem. 27 (1965) 801–808.
[15] K. Ohwada, J. Chem. Phys. 56 (1972) 4951.
[16] K. Ohwada, Inorg. Chem. 10 (10) (1971) 2281–2285.
[17] K. Ohwada, J. Inorg. Nucl. Chem. 32 (1970) 1209–1218.
[18] V.A. Volkovich, T.R. Griffiths, D.J. Fray, M. Fields, Vib. Spectrosc. 17 (1998) 83–91.
[19] V.A. Volkovich, T.R. Griffiths, D.J. Fray, R.C. Thied, Phys. Chem. Chem. Phys. 3 (2001) 5182–5191.
[20] R. Scholder, H. Gläser, Z. Anorg. Allg. Chem. 327 (1964) 15–27.
[21] J.-P. Marcon, O. Pesme, M. Franco, Rev. Int. Hautes Tempér. et Réfract. 9 (1972) 193–196.
[22] E.H.P. Cordfunke, D.J.W. IJdo, J. Solid State Chem. 115 (1995) 299–304.
[23] E.H.P. Cordfunke, B.O. Loopstra, J. Inorg. Nucl. Chem. 33 (1971) 2427–2436.
[24] D.J.W. IJdo, S. Akerboom, A. Bontenbal, J. Solid State Chem. 221 (2015) 1–4.
[25] A.L. Smith, P.E. Raison, L. Martel, T. Charpentier, I. Farnan, D. Prieur, C. Hennig, A. Scheinost, R.J.M. Konings, A.K. Cheetham, Inorg. Chem. 53 (1) (2014) 375–382.
[26] D. Bykov, P. Raison, R.J.M. Konings, C. Apostolidis, M. Orlova, J. Nucl. Mater. 457 (2015) 54–62.
[27] J.E. Battles, W.A. Shinn, P.E. Blackburn, J. Chem. Thermodyn. 4 (1972) 425–439.
[28] I. Jayanthi, V.S. Iyer, S.G. Kulkarni, G.A. Rama Rao, V. Venugopal, J. Nucl. Mater. 211 (1994) 168–174.
[29] R. Pankajavalli, V. Chandramouli, S. Anthonysamy, K. Ananthasivan, V. Ganesan, J. Nucl. Mater. 420 (2012) 437–444.
[30] A.L. Smith, J.-Y. Colle, O. Beneš, A. Kovacs, P.E. Raison, R.J.M. Konings, J. Chem. Thermodyn. 60 (2013) 132–141.
[31] J. Drowart, C. Chatillon, J. Hastie, D. Bonnell, Pure Appl. Chem. 77 (4) (2005) 683–737.
[32] P.E. Blackburn, P.M. Danielson, J. Chem. Phys. 56 (1972) 6156–6164.
[33] J.B. Mann, in: T. Hayakawa, K. Ogata (Eds.), Proceedings of the Conference on Mass Spectroscopy, Tokyo, University Park Press, Baltimore, MD, 1970.
[34] D.W. Bonnell, J.W. Hastie, Program SIGMA, A Fortran Code for Computing Atomic Ionisation Cross-sections, NIST, Gaithersburg, MD, unpublished work, 1990–1997.
[35] H.C. Straub, P. Renault, B.G. Lindsay, K.A. Smith, R.F. Stebbings, Phys. Rev. A 54 (3) (1996) 2146–2153.
[36] H. Deutsch, K. Becker, T.D. Märk, Int. J. Mass Spectrom. 167 (168) (1997) 503–517.
[37] J.W. Otvos, D.P. Stevenson, J. Am. Chem. Soc. 78 (1956) 546–551.
[38] R.T. Grimley, The Characterisation of High Temperature Vapors, John Wiley & Sons Inc, New York, 1967.
[39] R. Hultgren, R.L. Orr, P.D. Anderson, K.K. Kelley, Selected Values of Thermodynamic Properties of Metals and Alloys, John Wiley & Sons Inc, 1963.
[40] D.J. Santeler, J. Vac. Sci. Technol. A4 (3) (1986) 338–343.
[41] P. Gotcu-Freis, J.-Y. Colle, J.-P. Hiernaut, R.J.M. Konings, J. Chem. Thermodyn. 43 (2011) 492–498.
[42] F. Capone, J.-Y. Colle, J.P. Hiernaut, C. Ronchi, J. Phys. Chem. A 103 (1999) 10899–10906.
[43] D. Taylor, Br. Ceram. Trans. J 83 (1) (1984) 5–9.
[44] J.B. Berkowitz-Mattuck, A. Büchler, J.L. Engelke, S.N. Goldstein, J. Chem. Phys. 39 (1963) 2722–2730.
[45] B. McCarroll, J. Chem. Phys. 46 (1967) 863–869.
[46] C. Guéneau, A. Chartier, L. Van Brutzel, Compr. Nucl. Mater. 22–59 (2012).
[47] O. Beneš, R.J.M. Konings, J.-Y. Colle, J. Nucl. Mater. 462 (2015) 182–190.
[48] C. Guéneau, N. Dupin, B. Sundman, C. Martial, J.-C. Dumas, S. Gossé, S. Chatain, F. De Bruycker, D. Manara, R.J.M. Konings, J. Nucl. Mater. 419 (1–3) (2011) 145–167.
[49] D.L. Hildenbrand, E. Murad, J. Chem. Phys. 53 (1970) 3403.
[50] R.H. Lamoreaux, D.L. Hildenbrand, J. Phys. Chem. Ref. Data 13 (1984) 151–173.
[51] L.F. Malheiros, C. Chatillon, M. Allibert, High Temp. High Press. 20 (1988) 361–378.
[52] H.A. Wriedt, Bull. Alloy Phase Diagrams 8 (3) (1987) 234–246.
[53] R.J.M. Konings, O. Beneš, A. Kovacs, D. Manara, D. Sedmidubský, L. Gorokhov, V.S. Iorish, V. Yungman, E. Shenyavskaya, E. Osina, J. Phys. Chem. Ref. Data 43 (1) (2014).
[54] M. Binnewies, E. Milke, Thermochemical Data of Elements and Compounds, second ed., Wiley-VCH, 2002.
[55] E.H.P. Cordfunke, R.P. Muis, W. Ouweltjes, H.E. Flotow, P.A.G. O'Hare, J. Chem. Thermodyn. 14 (1982) 313–322.
[56] E.H.P. Cordfunke, B.O. Loopstra, J. Inorg. Nucl. Chem. 33 (1971) 2427–2436.
[57] M. Gasperin, J. Less Common Met. 119 (1986) 83–90.
[58] E.H.P. Cordfunke, P.A.G.O. Hare, The Chemical Thermodynamics of Actinide Elements and Compounds: 3. Pt. Miscellaneous Actinide Compounds, International Atomic Energy Agency, Vienna, 1978.
[59] T.C. Tso, D. Brown, A.I. Judge, J.H. Holloway, J. Fuger, J. Chem. Soc. Dalton Trans. (1985) 1853–1858.
[60] W.G. Lyon, D.W. Osborne, H.E. Flotow, H.R. Hoekstra, J. Chem. Thermodyn. 9 (1977) 201–210.
[61] O. Knacke, O. Kubaschewski, K. Hesselman, Thermochemical Properties of Inorganic Substances, second ed., Springer-Verlag, Berlin, 1991.
[62] C. Miyake, K. Fuji, S. Imoto, Chem. Phys. Lett. 46 (2) (1977) 349–351.
[63] C. Miyake, M. Kanamaru, H. Anada, S. Imoto, J. Nucl. Sci. Technol. 22 (8) (1985) 653–657.
[64] E.H.P. Cordfunke, W. Ouweltjes, J. Chem. Thermodyn. 13 (1981) 187–192.
[65] P.A.G. O'Hare, H.R. Hoekstra, J. Chem. Thermodyn. 6 (1974) 965–972.

JCT 15-191